International Journal of Mass Spectrometry 292 (2010) 53–63

Contents lists available at ScienceDirect

International Journal of Mass Spectrometry

journal homepage: www.elsevier.com/locate/ijms

Mass spectrometry (fragmentation ratios) of DNA base molecules following 80 keV proton impact with separation of direct ionization and electron capture processes

J. Tabet[a,b,c], S. Eden[a], S. Feil[a,b,c], H. Abdoul-Carime[a,b,c], B. Farizon[a,b,c,*], M. Farizon[a,b,c], S. Ouaskit[d], T.D. Märk[e]

[a] Université de Lyon, F-69003, Lyon, France
[b] Université Lyon 1, Villeurbanne, Lyon, France
[c] CNRS/IN2P3, UMR5822, Institut de Physique Nucléaire de Lyon, F-69622 Villeurbanne, France
[d] Laboratoire de physique de la matière condensée, Unité associée au CNRST (URAC 10), Faculté des sciences Ben M'sik, B.P.7955, Casablanca, Morocco
[e] Institut für Ionenphysik und Angewandte Physik, Leopold Franzens Universität, Technikerstrasse 25, A-6020 Innsbruck, Austria

ARTICLE INFO

Article history:
Received 25 September 2009
Received in revised form 8 March 2010
Accepted 9 March 2010
Available online 17 March 2010

Keywords:
DNA bases
Proton impact
Ionization
Electron capture
Mass spectrometry

ABSTRACT

The first fragmentation ratios are presented for the ionization of gas-phase DNA bases by 80 keV (1.8 v_0 in Bohr velocity units) proton impact. Event-by-event determination of the projectile charge state post-collision enables branching ratios to be determined for electron capture (EC) by the projectile and for direct ionization (DI) of the target molecule (without projectile neutralization). Results are compared with similar experiments on uracil [11] and water [14]. In all cases, whereas both processes (EC and DI) produce the same fragment ion groups, greater fragmentation ratios are observed for EC than for DI. Moreover the fragmentation ratio is greater for thymine than for adenine, cytosine, and uracil.

1. Introduction

Radiation-induced modification of DNA (deoxyribonucleic acid) leading to strand breaks and clustered lesions has long been recognized as a possible precursor for mutations and cancers in living systems [1]. More recently, a number of specific projectile–molecule interactions have been directly linked to the formation of DNA strand breaks [2]. These results have inspired extensive experimental and theoretical research on irradiation effects in isolated biomolecules with the aim to identify nano-scale processes leading to (multi-)fragmentation events in and around DNA. Although certainly not directly mirroring *in vivo*, the study of radiative interactions with gas-phase biomolecules enables diverse excitation, ionization, and dissociation processes to be observed directly, revealing detail, which cannot be extracted from experiments on condensed material. In particular, several recent studies have focused on proton collisions with gas-phase DNA bases, which may be considered to mimic interactions occurring during *proton therapies* [3–5]. In order to deliver localized doses of energy to destroy cells within tumors, these treatments exploit the *Bragg peak* maximum for energy deposition by incident protons with kinetic energies of about 100 keV (2.0 v_0 in Bohr velocity units, $v_0 = 2.19 \times 10^6$ ms^{-1}). The occurrence of the Bragg peak results from the interplay between ionization, excitation, and charge exchange processes as the projectiles slow down in the exposed tissue [6,7].

The present investigation is dedicated to proton interactions with the purine molecule adenine ($C_5H_5N_5$), and the pyrimidines cytosine ($C_4H_5N_3O$) and thymine ($C_5H_6N_2O_2$). Adenine and thymine form a Watson–Crick pair in DNA with two hydrogen bonds in the characteristic helical structure. Guanine, which pairs with cytosine via three hydrogen bonds in DNA, was not studied in the present investigation due to the reported difficulty of achieving a sufficiently high vapor pressure without isomerization and/or thermal decomposition [8]. Infra-red spectroscopy studies of adenine, thymine, and uracil [9] at 200–325 °C indicate that the tautomeric forms shown in Fig. 1 account for >99% of the sublimated molecules (uracil has been included in the figure in order to allow comparison as given in Section 3.3). Whereas gas-phase cytosine is typically present in the keto form, de Vries and co-workers' [10]

* Corresponding author at: Institut de Physique Nucléaire de Lyon, F69622 Villeurbanne, France.
E-mail address: bfarizon@ipnl.in2p3.fr (B. Farizon).

1387-3806/$ – see front matter © 2010 Elsevier B.V. All rights reserved.
doi:10.1016/j.ijms.2010.03.002

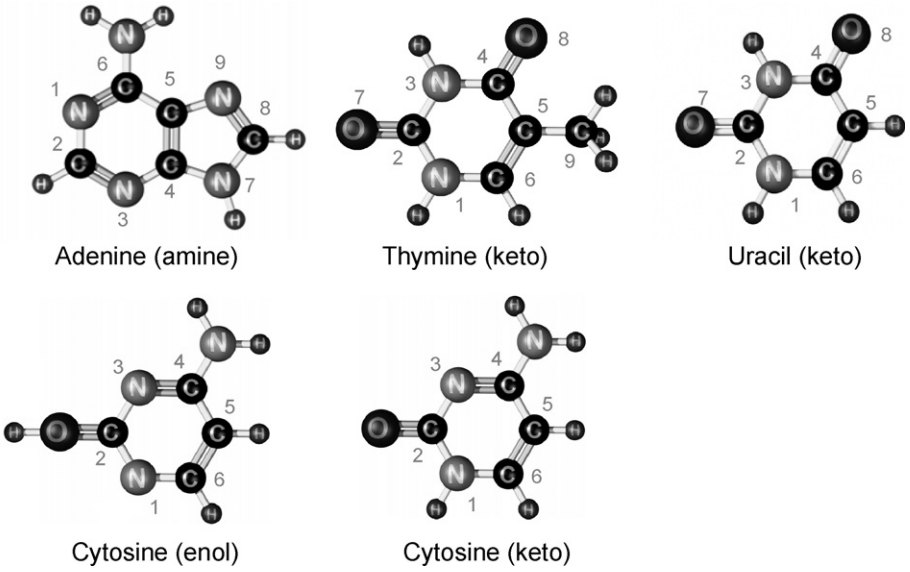

Fig. 1. Ground-state geometries of the dominant tautomeric forms of gas-phase adenine, thymine, uracil, and cytosine [9,10].

REMPI spectroscopic studies of laser-desorbed jet-cooled cytosine provided evidence for a significant additional population in the enol form characterized by an H atom bonding to the O atom instead of bonding at the N1 position (see Fig. 1).

The present work provides the first fragmentation patterns (mass spectra) for the ionization of gas phase DNA base molecules as a function of charge exchange between the projectile and target molecule (i.e., enabling electron capture processes to be distinguished from direct ionization reactions) at an impact velocity approximately coinciding with maximum energy deposition. To the authors' knowledge, the only previous measurements of this kind have been carried on uracil [11], O_2 [12], and H_2O [13–15]. Therefore, in addition to their potential use in nano-scale models of ion-induced radiation damage [16], the present results are of fundamental interest with respect to the production of fragment ions through electron capture (EC) and direct ionization (DI) in the case of electronically complex target molecules.

2. Experimental

The crossed-beam apparatus used for the present experiments is shown schematically in Fig. 2 and has been described in detail elsewhere [11,13,14]. Briefly, protons produced in a standard RF-gas discharge source (80 MHz) are accelerated to 80 keV with an energy resolution ($\Delta E/E$) of 0.01. The *primary* magnetic sector field is used to separate protons from other ions in the source (e.g., H_2^+ and H_3^+) and the background pressure is maintained below 10^{-6} Torr along the ensuing beamline. After collimation, the proton beam is crossed at right angles with an effusive target beam of DNA base molecules. The target beam is formed by the sublimation of adenine, cytosine, or thymine powder purchased from Sigma–Aldrich (minimum purity 99%) in a temperature-controlled Knudsen-type oven (±1 °C). In order to maximize statistics, measurements were recorded over a number of days and summed to generate the mass spectra and branching ratios presented Figs. 3–5 and Tables 1–5. The temperatures ranges of the present measurements are 130–171 °C for adenine, 168–186 °C for cytosine, and 125–133 °C for thymine. Previous high-resolution mass spectrometry and photoelectron spectroscopy studies of these molecules in similar conditions show no temperature dependence [8,9,17–20], indicating that thermal decomposition is not significant in the present experiments. Accordingly no temperature dependence is

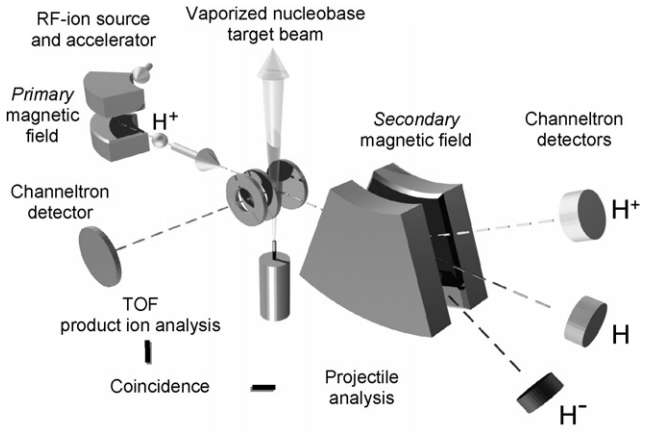

Fig. 2. Schematic diagram of the experimental system.

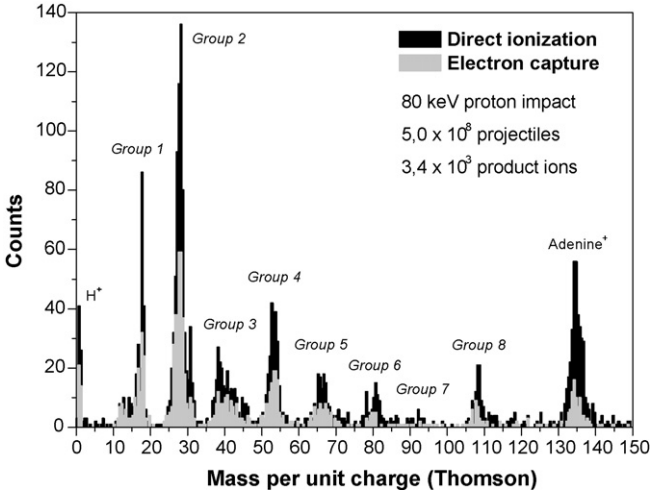

Fig. 3. Mass spectrum for proton impact ionization of adenine ($C_5H_5N_5$, 135 amu) by electron capture and by direct ionization at 80 keV. The main ions expected to account for the peaks are listed in Table 2.

Table 1
Electron capture ionization branching ratios and ionization energies for adenine, thymine, and cytosine following proton impact at 80 keV (1.8 v_0). The present results are compared with uracil [11] and water [14,15].

Molecule	Electron capture/total ionization (%)	Ionization energy (eV)	Main fragment cation appearance energy (eV)
Adenine	27.1 ± 4 (Present work)	8.20 ± 0.03 [21]	11.56 ± 0.05 ($C_4H_4N_4^+$, 108 Thomson) 12.8 ± 0.1 ($C_3H_3N_3^+$, 81) 13.1 ± 0.1 ($C_2H_4N_3^+$, 70) 13.2 ± 0.1 ($C_3H_2N_2^+$, 66) 13.7 ± 0.1 ($C_2H_2N_2^+$, 54) 13.0 ± 0.1 ($CH_3N_2^+$, 43) 14.0 ± 0.1 (CH_3N^+, 29) 13.1 ± 0.1 (CH_2N^+, 28) [21]
Cytosine	27.6 ± 4 (Present work)	8.45 [22][c]	Unmeasured 10.70 ± 0.05 ($C_4H_5NO^+$, 83) 13.20 ± 0.05 ($C_4H_4NO^+$, 82) 11.7 ± 0.1 ($C_3H_5N^+$, 55) 11.9 ± 0.1 ($CHNO^+$, 43) 14.4 ± 0.1 ($C_3H_3^+$, 39) 13.6 ± 0.1 (CH_2N^+, 28) [21]
Thymine	26.6 ± 4 (Present work)	8.82 ± 0.03 [21]	10.95 ± 0.05 ($C_3H_3NO^+$, 69) 13.40 ± 0.05 ($C_3H_2NO^+$, 68) 13.6 ± 0.2 ($CHNO^+$, 43) 13.25 ± 0.05 ($C_2H_2O^+$, 42) 12.95 ± 0.05 ($C_2HO^+/C_2H_3N^+$, 41) 14.06 ± 0.10 ($C_2H_2N^+$, 40) 13.75 ± 0.05 (CH_2N^+, 28) [21]
Uracil	25.4 ± 2 [11][a]	9.15 ± 0.03 [21]	18.08 ± 0.05 (OH^+) [24] 19.0 (O^+)[c] [25] 19.65 ± 0.05 (H^+) [24]
Water	27.8 ± 2 [14][a,b] 25.7 [15][c]	12.621 ± 0.002 [23]	

[a] Measured with the same experimental system used to obtain the present results.
[b] This result was corrected for differences in TOF transmission for the different product ions. As the relative production of fragment ions at this impact energy is greater for EC than for DI, correcting for acceptance tends to increase %EC results.
[c] No error estimation available.

apparent in the present mass spectra, although the sensitivity to detect such effects is limited by low statistics prior to summing data recorded on different days.

The charge state of the projectile after a collision with a nucleobase molecule is determined using the secondary magnetic sector field analyzer with three channeltron detectors located at the appropriate positions to detect H^+, H^0 and H^-. A compact linear time-of-flight (TOF) mass spectrometer is used to analyze the product ions formed by the collision of a proton with a DNA base molecule. The detection of the projectile after its interaction with a target molecule provides the reference time for the time-of-flight determination of the mass-to-charge ratio of the product ions (resolution ≈20 Thomson). By simultaneously determining the mass-per-charge ratio of the product ions and the post-interaction charge of the projectile, the experiment enables *direct ionization* (product ion detection with coincident H^+ detection after the secondary magnetic analyzer) to be distinguished from *electron capture* (coincident H^0 detection) for each ionizing collision. Thus, in the present terminology, direct ionization (DI, Eq. (1) below) describes the removal of an electron from the nucleobase molecule without projectile neutralization, and electron capture (EC, Eq. (2)) describes the transfer of an electron from the nucleobase molecule to the projectile. In Eqs. (1) and (2), *the ionized target system* refers to the (often metastable) nucleobase ion or the (fragment ion + neutrals) which result from its dissociation.

$$H^+ + \text{nucleobase} \rightarrow H^+ + e^- + (\text{theionizedtargetsystem}) \quad (1)$$

$$H^+ + \text{nucleobase} \rightarrow H^0 + (\text{theionizedtargetsystem}) \quad (2)$$

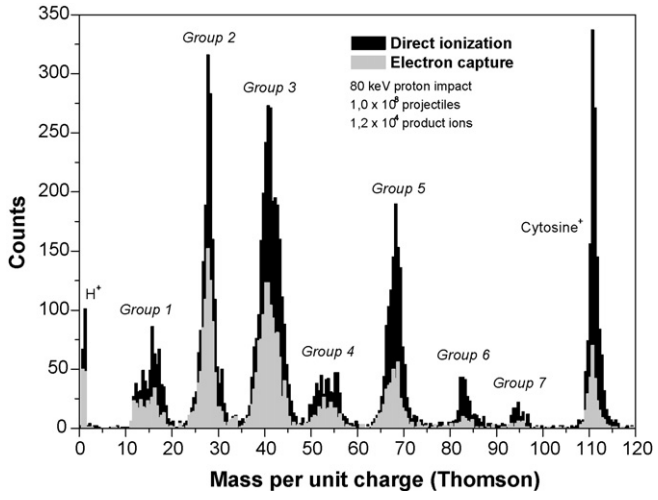

Fig. 4. Mass spectrum for proton impact ionization of cytosine ($C_4H_5N_3O$, 111 amu) by electron capture and by direct ionization at 80 keV. The main ions expected to account for the peaks are listed in Table 3.

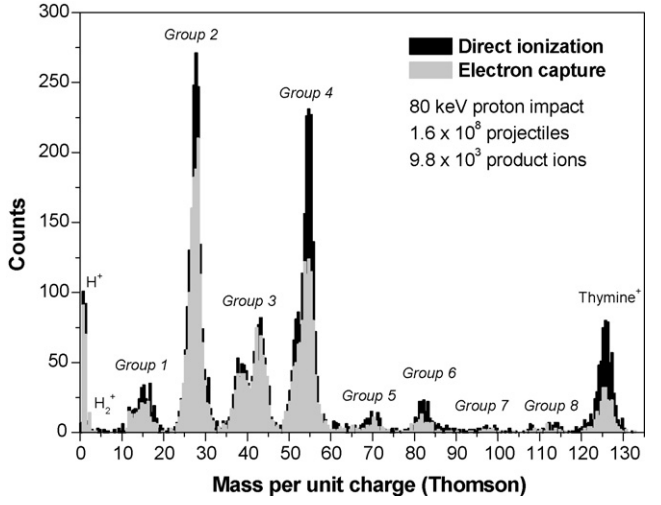

Fig. 5. Mass spectrum for proton impact ionization of thymine ($C_5H_6N_2O_2$, 126 amu) by electron capture and by direct ionization at 80 keV. The main ions expected to account for the peaks are listed in Table 4.

Table 2
Product ions observed following the ionization of gas-phase adenine by photon absorption [21], electron impact [26], and proton impact (present work).

m/*q* in Thomson (with previous ion sum formula proposals)		
Ionization by 80 keV proton impact (present work)[a,b,c,d]	Ionization by 70 eV electron impact[e] [26]	20 eV photo-ionization (with proposed ion formula)[e] [21]
134–136 (peak 135)	135 134 – *weak* 120 – *weak*	135 (adenine$^+$) 134 ($C_5H_4N_5^+$) 120 ($C_5H_4N_4^+$) – *weak* 119 ($C_5H_3N_4^+$) – *weak*
107–109 (peak 109)	108 107 – *weak*	108 ($C_4H_4N_4^+$) 107 ($C_4H_3N_4^+$) 92 ($C_4H_2N_3^+$)
78–82 (peak 81)	81 80 70	81 ($C_3H_3N_3^+$) 80 ($C_3H_2N_3^+$) 70 ($C_2H_4N_3^+$)
64–68 (peak 66)	67 66 65	67 ($C_3H_3N_2^+$) 66 ($C_3H_2N_2^+$) 65 ($C_3HN_2^+$) – *weak*
52–54 (peak 53)	54 53	54 ($C_2H_2N_2^+$) 53 ($C_2HN_2^+$)
37–42 (full range 36–47, peak 38)	43 42 – *weak* 41 – *weak* 40 39 38	43 ($CH_3N_2^+$) 42 ($CH_2N_2^+$) 41 (CHN_2^+) 40 (CN_2^+) – *weak* 39 (C_2HN^+) – *weak* 38 (C_2N^+) – *weak*
30–31 (peak 31: $N_2H_3^+$)		
27–29 (peak 28)	29 28 27	29 (CH_3N^+) 28 (CH_2N^+) 27 (CHN^+)
18 (H_2O^+ impurity)		18 (H_2O^+) – *weak*
17 (OH^+ impurity)		17 (NH_3^+/OH^+) – *weak*
Full range 12–16 (C^+, CH^+, N^+, NH^+, NH_2^+)	Not measured	
		14 (N^+) – *weak*
1 (H^+)		Not measured

[a] The same peak positions were observed for both direct ionization and electron capture.
[b] Unless stated otherwise, the ranges given above correspond to the half-maximum width of the DI peaks.
[c] The proton impact data only includes single ion production.
[d] Possible assignments for previously unobserved peaks.
[e] The channels labeled *weak* correspond to those reported by Jochims et al. [21] and Rice and Dudek [26] to have intensities <5% of the maximum peak intensity.

The results presented in Section 3 correspond to single ion production only; events involving the detection of two or more fragment ions in coincidence with a single projectile are not included here. Similarly, due to the relatively poor statistics, this paper does not present results for double ion production events, double electron capture events, and events involving both projectile neutralization and electron emission.

3. Results and discussion

3.1. Branching ratios for electron capture

Branching ratios for electron capture in 80 keV collisions with adenine, cytosine, and thymine over total ionization (summed EC plus DI) are presented in Table 1. The table also lists EC branching ratios derived from recent proton impact experiments on uracil [11] and water [14,15], as well as the appearance energies for the major ions given in the literature. The measured EC branching ratios for adenine, cytosine, thymine, and uracil lie within each other's error limits, as may be expected considering the broadly similar compositions, geometries, and ionization energies of the three molecules. Moreover, the close agreement of the nucleobase results with the water results suggests that the lowest ionization energy is not a decisive factor influencing of the ratio of EC to DI events in 80 keV proton collisions with these molecules. Indeed the intense production of fragment ions shown in Figs. 3–5 and Tables 2–5 (e.g., fragmentation ratio of 94% for EC in 80 keV proton collisions with thymine) suggests that the removal of electrons from valence orbitals other than the HOMO may contribute significantly to the present data.

3.2. 80 keV proton impact mass spectra

3.2.1. Adenine

Fig. 3 shows the mass spectrum for single ion production by electron capture and direct ionization in collisions between gas-phase adenine molecules and 80 keV (1.8 v_0) protons. Groups 1–8 correspond to the production of fragment ions containing 1–8 of the *heavier atoms* C or N. Although the relative production of fragment ions is different for direct ionization and electron capture (see Section 3.3), peaks at the same m/q values are observed for both processes (Table 2).

The studies of Schlathölter et al. [27,28] and Brédy et al. [29] on gas-phase adenine provide the only previous measurements of fragment ion production with $m/q < 12$ Thomson. Schlathölter et al. [27,28] report TOF mass spectra for 0.26 v_0 C^+ (singly charged carbon ions at 0.26 Bohr velocities), 0.45 v_0 He^{2+}, 0.47 v_0 C^{5+}, and 0.35 v_0 O^{5+} impact. For single electron capture by incident 0.28 v_0 F^{2+} projectiles, Brédy et al.'s [29] coincidence experiments probe electron emission with cation production. The present data show significant production of H^+ but provides no evidence for ions in the range 2–11 Thomson attributable to H_2^+ or *small* doubly charged

fragments. The only previous singly charged ion (C^+) impact mass spectrum covering this m/q range shows weak H_2^+ production but no peaks for doubly charged ions [27]. Conversely, the previous mass spectra for 0.45 v_0 He^{2+} impact [27], for 0.47 v_0 C^{5+} [28] impact, and for double or triple ionization upon 0.28 v_0 F^{2+} impact [29] demonstrate quite significant ion signals between the major peaks at 1 and 12 Thomson. The 0.35 v_0 O^{5+} impact mass spectrum shows quite clear peaks at 2 and 4–8 Thomson [27]. The production of doubly charged fragment ions by multiply charged ion impact can be attributed to greater projectile charge states increasing the probability of multiple electron capture. Moreover, the strong fields around multi-charged ions enable electron capture to take place in collisions with relatively large impact parameters (more distant interactions), associated with lower energy transfer [30]. Hence increased H_2^+ production by multi-charged ion impact may be explained by the formation of relatively stable excited parent

Table 3
Product ions observed following the ionization of gas-phase cytosine by 80 keV (present work) and 100 keV [5] proton impact and by 70 eV electron impact [37].

m/q in Thomson			Suggested ion sum formulae (principle peak assignments in bold)
70 eV electron impact[a] [37]	100 keV proton impact[c] [5]	80 keV proton impact[b,d,e] (present work)	
111	111	110–111 (peak 111)	**$C_4H_5N_3O^+$** (cytosine$^+$), $C_4H_4N_3O^+$
110 – *weak*			
95	95	93–96 (peak 95)	**$C_4H_3N_2O^+$**, $C_4H_5N_3^+$, $C_4H_2N_2O^+$, $C_4H_4N_3^+$
94 – *weak*			
84 – *weak*		82–84 (peak 83)	$C_2H_2N_3O^+$, $C_4H_5NO^+$, $C_2HN_3O^+$, **$C_3H_5N_3^+$**, $C_3H_4N_3^+$, $C_2N_3O^+$
83	83		
82 – *weak*			
70 – *weak*		66–70 (peak 68)	$C_2H_2N_2O^+$, $C_3H_3NO^+$, $C_3H_5N_2^+$, **$C_3H_2NO^+$**, **$C_3H_4N_2^+$**, $C_2N_2O^+$, $C_3H_3N_2^+$, $C_3H_2N_2^+$
69	69		
68	68		
67	67		
66	66*		
65 – *weak*			
57 – *weak*		50–57 (peaks at 53 and 55)	CN_2O^+, $C_2H_2NO^+$, **$C_2H_3N_2^+$**, $C_3H_4N^+$, **$C_3H_3N^+$**, $C_3H_2N^+$, C_3HN^+
56	56*		
55	55		
54 – *weak*			
53	53*		
52	52		
51	51*		
45 – *weak*			
44	44		
43	43	39–43 (peak 41)	$CHNO^+$, CNO^+, $CH_2N_2^+$, $C_2H_4N^+$, CHN_2^+, **$C_2H_3N^+$**, $C_2H_2N^+$, CN_2^+, C_2HN^+
42	42		
41	41		
40	40		
39	39		
38	38		
37 – *weak*			
32 – *weak*	32*		
	31*		
29	29		CH_3N^+, CHO^+, **CH_2N^+**, CO^+, CHN^+, $C_2H_2^+$
28	28	27–29 (peak 28)	
27	27*		
26	26*		
25 – *weak*	25*		
	18*	Full range 12–18 (peak 16)	
	17		
	16*		
Not measured[f]	15		H_2O^+ (impurity), OH^+, **NH_2^+**, O^+, NH^+, N^+, C^+,
	14		
	13		
	12		
	Not measured	1	H^+

[a] The channels labeled *weak* correspond to those reported by Rice et al. [37] to have intensities <5% of the maximum peak intensity.
[b] The same peak positions were observed for both direct ionization and electron capture.
[c] The non-asterisked product ion masses were labeled or mentioned explicitly by Le Padellec et al. [5]. Conversely, the asterisked masses have been read from a published figure and are therefore subject to greater uncertainty.
[d] Unless stated otherwise, the ranges given above correspond to the half-maximum width of the DI peaks.
[e] The present proton impact data only includes single ion production.
[f] The 70 eV electron impact mass spectrum shown on the NIST database [23] includes ions in the range 12–18 Thomson.

Table 4
Product ions observed following gas-phase thymine ionization by photon absorption [21], by 70 eV electron impact [37,39], and by 100 keV [5] and 80 keV proton impact (present work).

m/*q* in Thomson (with previous ion sum formula proposals)				
Proton impact 80 keV[a,b,c,d] (present work)		70 eV electron impact 100 keV[e] [5]		20 eV photo-ionization[f] [21] [39]
		128		
125–127 (peak 126)		127		
	126	126 Thymine$^+$	126	126 Thymine$^+$ ($C_5H_6N_2O_2^+$)
		125		125 ($C_5H_5N_2O_2^+$) – *weak*
		124		
108–114 (peak 112) $C_4H_4N_2O_2^+$, $C_4H_3N_2O_2^+$		112		
95–100 (peak 98)	97*	97	97 – *weak*	97 ($C_4H_3NO_2^+$) – *weak*
80–84 (peak 82)		84	84 – *weak*	84 ($C_4H_6NO^+$) – *weak*
	83*	83 ($C_4H_5NO^+$)	83	83 ($C_4H_5NO^+$)
	82	82 ($C_4H_4NO^+$)	82	82 ($C_4H_4NO^+$)
		81		
		80		
68–72 (peak 70)	71*	71	71 – *weak*	71 ($C_2HNO_2^+$) – *weak*
	70*	70	70 – *weak*	70 ($C_2H_2N_2O^+$) – *weak*
				58 (unassigned) – *weak*
53–56 (full range 49–59, peak 55)		56	56	56 ($C_3H_4O^+$)
	55	55 ($C_3H_5N^+$)	55	55 ($C_3H_5N^+$)
	54	54 ($C_3H_4N^+$)	54	54 ($C_3H_4N^+$)
		53	53	53 (unassigned) – *weak*
	52	52	52	52 (unassigned) – *weak*
41–45 (peak 43)		45		45 (unassigned) – *weak*
	44	44 (CH_2NO^+)	44	44 (CO_2^+ impurity)
	43	43	43 – *weak*	43 ($CHNO^+$) – *weak*
	42*	42		
		41	41 – *weak*	41 (unassigned) – *weak*
37–40 (peak 39)	40	40 ($C_3H_4^+/CN_2^+$)	40	40 ($C_3H_4^+$)
	39	39 ($C_3H_3^+$)	39	39 ($C_3H_3^+$)
	38	38 ($C_3H_2^+$)	38 – *weak*	
		37 (C_3H^+)	37 – *weak*	
26–29 (peak 28)	29	29	29 – *weak*	29 (unassigned) – *weak*
	28 (CH_2N^+/CO^+)	28 (CH_2N^+/CO^+)	28	28 (CH_2N^+)
	27*	27 ($C_2H_3^+/CHN^+$)	27	27 ($C_2H_3^+/CHN^+$)
	26*	26 ($C_2H_2^+$)	26	26 ($C_2H_2^+$) – *weak*
	25*	25 (C_2H^+)		
18	18*	18 (H_2O^+)		
12–17 (peak 15)	17 (OH^+)	17 (OH^+)		
	16*	16 (CH_4^+/O^+)		
	15 (NH^+)	15 (CH_3^+)		
	14 (N^+)	14 (CH_2^+)	Not measured	Not measured
	13 (CH^+)	13 (CH^+)		
	12 (C^+)	12 (C^+)		
2	Not measured	2 (H_2^+)		
1		1 (H^+)		

[a] The same peak positions were observed for both direct ionization and electron capture.
[b] Unless stated otherwise, the given ranges correspond to the half-maximum width of the DI peaks.
[c] The proton impact data only includes single ion production.
[d] Ion formula proposals are given for previously unobserved or unassigned peaks.
[e] The non-asterisked product ion masses were labeled or mentioned explicitly by Le Padellec et al. [5]. Conversely, the asterisked masses have been read from a published figure and are therefore subject to greater uncertainty (the feature centered 97 Thomson is particularly weak and uncertain).
[f] The channels labeled *weak* correspond to those reported by Jochims et al. [21] and Rice et al. [37] to have intensities <5% of the maximum peak intensity.

ions in large-impact-parameter interactions enabling more nuclear rearrangements to occur as the system relaxes prior to fragmentation. It should be noted that electron capture processes dominate in the velocity range studied by Schlathölter et al. [27,28] and Brédy et al. [29] (0.26–0.47 v_0) and that the impact parameters for the presently observed EC interactions at 1.8 v_0 can be assumed to be significantly smaller.

For 0.28 v_0 F^{2+} collisions with gas-phase adenine, Brédy et al. [29] report the number of electrons emitted from the molecule in single-EC events. A small peak at 18 Thomson, attributable to NH_4^+ fragments or to the ionization of H_2O impurities, occurs in the mass spectrum for single electron capture without electron emission [29]. However, no equivalent peak is apparent for single electron capture with the emission of 1, 2, or 3 electrons. In these mass spectra, only single EC with zero electron emission can produce peaks at *m*/*q* corresponding to the *parent* ion (adenine or an impurity). Therefore, the disappearance of the 18 Thomson peak for electron capture with electron emission [29] implies that it is attributable to non-dissociative ionization of H_2O. The low background pressure (10^{-8} mbar) in Brédy et al.'s [29] experiments indicates that any significant impurity must have been due to the target jet. Although heating to 130 °C [29] (upto 171 °C in the present work) would generally be expected to remove water from the sample prior to measurements, long periods of degassing may be required to remove water trapped within grains of the nucleobase powder (as observed for uracil by Abouaf and Dunet [31]). In the present work, while background measurements provide no evidence for water, Fig. 3 includes a major peak at 18 Thomson. The relative intensity of the 18 Thomson peak varies significantly for the five separate measurements, which are summed to form this mass spectrum. This variation may be attributed to differences in heating times and temperatures leading to more or less effective water removal from the sample prior to the experiments. Therefore, the 18 Thomson peak in Fig. 2 is assigned primarily to H_2O impurities in the sample

Table 5
Product ion fragmentation ratios (the number of ions detected in a given m/q range over the total number of ions detected) for 80 keV proton collisions with gas-phase adenine, thymine, cytosine, and uracil [11]. Background noise has been removed and the ions produced by electron capture (EC) and by direct ionization (DI) have been given separately.

Molecule	% (fragment ion production/total ionization)											
	H^+		H_2^+		Group 1 $10 \le m/q < 20$[a]		Group 2 $20 \le m/q < 35$		Group 3 $35 \le m/q < 47$		Group 4 $47 \le m/q < 60$	
	EC	DI	EC	DI	EC	DI	EC	DI	EC	DI	EC	DI
Adenine (M = 135)	3.3 ± 0.6	2.7 ± 0.7	0.0 ± 0.1	0.1 ± 0.2	14.6 ± 1.3	10.9 ± 1.4	32.1 ± 2.1	28.9 ± 2.5	12.2 ± 1.2	10.8 ± 1.3	12.5 ± 1.2	10.7 ± 1.2
Thymine (M = 126)	4.1 ± 0.3	3.4 ± 0.6	0.5 ± 0.1	0.3 ± 0.2	4.9 ± 0.4	5.1 ± 0.7	32.8 ± 1.0	28.5 ± 1.7	19.9 ± 0.8	15.7 ± 1.0	26.7 ± 0.9	29.0 ± 1.6
Cytosine (M = 111)	2.9 ± 0.3	1.9 ± 0.2	0.0 ± 0.1	0.0 ± 0.1	8.5 ± 0.5	7.6 ± 0.6	25.1 ± 1.0	19.5 ± 0.8	33.9 ± 1.2	29.7 ± 0.9	6.9 ± 0.5	6.4 ± 0.4
Uracil[b] (M = 112)	2.7 ± 0.3	1.5 ± 0.3	0.0 ± 0.1	0.0 ± 0.1	6.9 ± 0.6	5.0 ± 0.5	24.9 ± 1.1	22.3 ± 1.0	40.2 ± 1.5	37.5 ± 1.0	3.6 ± 0.4	2.9 ± 0.3

Molecule	% (fragment ion production/total ionization)											
	Group 5 $60 \le m/q < 75$		Group 6 $75 \le m/q < 90$		Group 7 $90 \le m/q < 105$		Group 8 $105 \le m/q < 115$		M^+ group	
	EC	DI	EC	DI	EC	DI	EC	DI	EC	DI
Adenine (M = 135)	7.5 ± 0.9	6.8 ± 1.0	3.2 ± 0.6	4.7 ± 0.8	1.2 ± 0.4	1.0 ± 0.5	3.8 ± 0.6	4.8 ± 0.7	8.4 ± 1.0	17.2 ± 1.6
Thymine (M = 126)	2.0 ± 0.2	2.5 ± 0.5	2.2 ± 0.2	3.4 ± 0.5	0.4 ± 0.1	0.7 ± 0.3	0.6 ± 0.1	1.1 ± 0.3	5.9 ± 0.4	10.7 ± 0.8
Cytosine (M = 111)	11.5 ± 0.6	14.7 ± 0.6	2.1 ± 0.3	3.5 ± 0.3	1.0 ± 0.2	1.5 ± 0.2	–		8.1 ± 0.5	15.1 ± 0.6
Uracil[b] (M = 112)	11.2 ± 0.7	14.2 ± 0.7	0.6 ± 0.2	0.7 ± 0.2	0.2 ± 0.1	0.2 ± 0.2	–		9.6 ± 0.7	15.5 ± 0.7

The errors given in the table are purely statistical; the transmission of the TOF mass spectrometer has not been taken into account. Group m/q ranges are given in Thomson. M, nucleobase mass in amu. For all the nucleobases, no evidence was observed for fragment ion production above the background noise for masses in the range $2.5 < m/q < 10$ Thomson. For adenine, no evidence was observed for fragment ion production above the background noise for masses in the range $115 < m/q < 125$ Thomson.

[a] This group may contain contributions due to water impurities in the jet. In particular, this is expected to account for the high ion yields in this range for adenine.

[b] Tabet et al. [11].

jet. Similarly, the 17 Thomson peak is assigned to a combination of NH_3^+ production from adenine and OH^+ from H_2O.

In the present measurements, slightly stronger ion production is observed at 12 and 13 Thomson (C^+ and CH^+) than at 14 and 15 Thomson (N^+ and NH^+, although CH_2^+ and CH_3^+ may also contribute). The mass spectrum reported by Schlathölter et al. [27] for the ionization of gas-phase adenine in 0.26 v_0 collisions with C^+ projectiles also shows greater production of C^+ than N^+. Conversely, Brédy et al. [29] report negligible C^+ production but strong N^+ production for single electron capture from adenine without electron emission. As the present results include only single ion production channels, this difference with Brédy et al.'s [29] *zero electron emission* results are quite surprising. However, it can be rationalized by considering that whereas N^+ can be produced by breaking one C–N and two N–H bonds, or one C–N and one C=N bond, C^+ production involves breaking one double bond (C=C or C=N) and two single bonds (C–C, C–N, or C–H). Therefore, C^+ production is expected to require greater energy transfer, generally associated with smaller impact parameters (more *direct* collisions). Accordingly, increased relative C^+ production is reported by Brédy et al. [29] for electron capture with single, double, and triple electron emission, corresponding to interactions with successively smaller impact parameters. Similarly, the relatively intense C^+ production observed here is consistent with the fact that the impact parameters for single electron capture without electron emission are much greater in Brédy et al.'s [29] slow (0.28 v_0) doubly charged ion impact experiments than in the present fast (1.8 v_0) proton-molecule collisions.

For product ions ≥20 Thomson, Alvarado et al. [32] report mass spectra for 0.75 v_0 H^+, 0.37 v_0 He^+, and 0.22 v_0 C^+ collisions with gas-phase adenine and draw comparisons with equivalent neutral projectile impact results (H^0, He^0, and C^0). The same main groups of product ions are observed in the present and previous experiments [27–29]. However, whereas groups 7 and 9 are weak but visible in Schlathölter et al.'s [27] 0.26 v_0 C^+ impact result and in Jochims et al.'s [21] 20 eV photo-ionization mass spectrum, they are not discernable in Fig. 3 (although Table 5 shows that ion production in group 7 was marginally higher than the background noise) or in the data of Alvarado et al. [32], Brédy et al. [29], and Schlathölter et al. [28]. The weak production of fragment ions >115 Thomson is consistent with Leach and co-workers' [21,33] inference that fragmentation following photo-ionization originates from metastable $(adenine^+)^*$ with the positive charge (*hole*) localized on the NH_2 group. Accordingly, NH_2^+ production is expected to dominate single ionization involving the removal of one C or N but leaving the *double ring* structure intact, while the removal of an atom from within the double ring will generally cause multi-fragmentation.

The group maxima observed by Schlathölter et al. [27] are consistent with the present data, while minor differences in peak positions of the heavier fragment ions may be due to the relatively low resolution of the present data. Table 2 compares the ion masses observed in the present work with those reported by Rice and Dudek [26] for 70 eV (2.3 v_0) electron impact and by Jochims et al. [21] for 20 eV photo-ionization. The assignments proposed by the previous authors are generally consistent, with the exception of the peak at 53 Thomson, which is attributed to $C_3H_3N^+$ and $C_2HN_2^+$ by Brédy et al. [29] and Jochims et al. [21], respectively. The principle pathway identified in the literature is based on the sequential loss of HCN groups, while electron impact studies of variously labeled adenine derivatives [34–36] suggest that dissociation along the C(2)–N(3) and N(1)–C(6) bonds dominates (see Fig. 1). The work of Jochims et al. [21] provides a thorough review of adenine fragmentation pathways and predicts significant bond rearrangements in the key metastable cations prior to fragmentation.

Alvarado et al. [32] report clear evidence for the production of $adenine^{2+}$ (67.5 Thomson) in all of their ion and neutral impact

studies. This demonstrates an unusually high stability of the doubly charged adenine ion and leads us to expect its production to contribute to the present results. However, the mass resolution of the present spectrum is insufficient to separate evidence for adenine^{2+} from ion production at 67 and 68 Thomson, also clearly observed by Alvarado et al. [32].

Alvarado et al.'s [32] high-resolution TOF data also reveal shifts in peak positions away from integer values of m/q which were attributed to sequential fragmentation events occurring in the field-free region between the extraction and reflectron parts of the mass spectrometer. Although it is not possible to observe these effects in the present lower resolution linear TOF experiments, Alvarado et al.'s [32] analysis highlights that the stability of excited ionic states may lead to significant differences between different adenine mass spectrometry experiments. In particular, the high-energy deposition expected under the present ionizing conditions is expected to lead to (adenine$^+$)* production in highly excited states and thus the observation of only a few *parent* and large fragment ions (see Section 3.3).

3.2.2. Cytosine

The mass spectra for single ion production through electron capture and direct ionization in 80 keV proton collisions with gas-phase cytosine molecules is shown in Fig. 4. The same peak positions are observed for both ionizing processes (Table 3).

To the authors' knowledge, the only previous cytosine fragment ion measurements available in the literature are reported for 12 and 70 eV electron impact [23,37] and for 100 keV proton impact [5]. In addition, ion and cluster ion production mass spectra are available for 10 and 13 eV electron interactions with supersonic jets comprising cytosine and a carrier gas (He, Ar, H_2O, or a mixture of these gases) [38]. Kim et al. [38] report that the strongest peaks correspond to multiples of 109 Thomson and propose that this provides evidence that cytosine loses two hydrogen atoms upon *modest heating*. Conversely, the present results show a local maximum at 111 Thomson and no clear evidence for ion production at 109 Thomson, in agreement with the previous mass spectra for gas-phase cytosine [5,23,37]. Furthermore, the intensity of the peak at 112 Thomson in Rice et al.'s [37] high-resolution mass spectrum is ~10% of the peak at 111 Thomson, consistent with the molecular weight of 111.10 listed in the NIST database [23]. This strongly suggests that uracil *impurities* or protonated cytosine do not contribute significantly to the present data. We suspect that the relatively complex peak structure between 108 and 113 Thomson in Kim et al.'s [38] electron impact mass spectrum may be due to the ionization and subsequent break-up of clusters containing cytosine molecules, as opposed to heating effects on monomers. This rationale also implies that the target jet for the present experiments does not contain a significant density of cytosine dimers or larger clusters.

The mass spectra for high-energy ($\gg$IE) electron impact and 100 keV proton impact on cytosine [5,23,37] show the same major groups of product ions as observed in the present data. The peak positions in the present and previous mass spectra are listed in Table 3 [5,37] and the proposed assignments are broadly consistent with Rice et al.'s [37] discussion of dissociative ionization pathways. All the possible product ion groups (group 0 for H^+ fragments through to group 8 for cytosine$^+$) are clearly present in the cytosine mass spectrum. The strong production of large fragment ions implies that a significant proportion of dissociative ionization events originate from (cytosine$^+$)* with the positive charge (hole) localized on the central C_4N_2 ring. This is consistent with Jochims et al.'s [21] association of uracil and thymine dissociative ionization with metastable precursors characterized by hole localization on the N(1) atom (Fig. 1). Accordingly, Rice et al. [37] suggest the removal of the neutral amino group (NH_2) as the first step in one of three major fragmentation pathways for ionized cytosine, thus accounting for the peak at 93 Thomson. The next step in this proposed pathway is the expulsion of HCN, associated with the 68 Thomson peak.

The second pathway proposed by Rice et al. [37] for the dissociative ionization of cytosine begins with CO expulsion (accounting for the peak at 83 Thomson) followed by HCN loss (leaving an ion of 56 Thomson). Retro Diels–Alder reactions are suggested [37] as the third main pathway beginning with the expulsion of NCO or HNCO, possibly preceded by H loss (leaving ions of 67–69 Thomson). The next step is HCN expulsion, corresponding to ion production at 40–42 Thomson. The present difference of 27 Thomson (HCN) between the local maxima of these groups (68 and 41 Thomson) appears to be consistent with this proposed sequence.

Whereas only the lowest ionization energy of cytosine is available in the literature (8.45 eV [21], Table 1), an indication of fragment ion appearance energies is provided by Rice et al.'s [37] 12 eV electron impact mass spectrum, which shows peaks at 68, 69, 83, 84 (very weak), 111, and 112 Thomson. The only peaks in the photo-ionization mass spectra of thymine and uracil [21] which have appearance energies below 12 eV by more than a few tenths of an eV (see Table 1) occur at 83 and 69 Thomson. The 83 Thomson peak in the thymine spectrum is assigned to $C_4H_5NO^+$ by Jochims et al. [21]. For cytosine, $C_4H_5NO^+$ production would require significant atomic rearrangement prior to fragmentation or the removal of the double-bonded N(3) atom from the ring (see Fig. 1). Therefore, Rice et al.'s [37] $C_3H_5N_3^+$ assignment (CO loss) seems the most probable for the 83 Thomson peak in the cytosine mass spectrum, although $C_2HN_3O^+$ production via the cleavage of the N(1)–C(6), the C(4)–C(5), and two N–H single bonds may also contribute. At 69 Thomson, Jochims et al.'s [21] assignment of the peak in the uracil mass spectrum to $C_3H_3NO^+$ production represents a plausible alternative to Rice et al.'s [37] $C_3H_5N_2^+$ (NCO loss) proposal for the corresponding peak in the cytosine data. $C_3H_3NO^+$ can be formed from both cytosine and uracil without any atomic rearrangement or double bond breaking prior to dissociation.

Le Padellec et al. [5] provide the only previous fragment ion assignments below the major peak centered at 41 Thomson in the cytosine mass spectrum (100 keV proton impact: C^+, CH^+, N^+, NH^+ and OH^+ in group 1, and CH_2N^+ or CO^+ for the peak at 28 Thomson). The present assignments are based primarily on analogies with the other nucleobases. All three DNA bases discussed here and uracil [11] feature strong peaks at 28 Thomson. It is also worth noting that the appearance energies for the 28 Thomson ions (not available for cytosine) are close to each other, i.e., 13.1 ± 0.1 eV for adenine, 13.6 ± 0.1 eV for thymine, and 13.75 ± 0.05 eV for uracil [21]. These similar appearance energies suggest that this peak may be associated with similar fragment ions for these nucleobases. As oxygen is not present in adenine, this implies that CO^+ and COH^+ product ions may contribute relatively weakly to the peak centered at 28 Thomson in the cytosine mass spectrum. This appears to be consistent with the major role of HCN expulsion in Rice et al.'s [37] description of sequential fragmentation following cytosine ionization and with the expected localization of the metastable cytosine cation's positive charge (hole) on the N(1) atom. However, electron impact ionization experiments on deuterated thymine in the gas phase [39] indicate that CO^+ may also contribute to the thymine mass spectrum. Accordingly we assign the cytosine group 2 primarily to CNH_n^+ ($n = 1$–3) production, in general agreement with Jochims et al.'s [21] assignments for 20 eV photo-ionization of gas phase uracil and thymine, with weaker contributions from CO^+ and $C_2H_n^+$.

In the 10–20 Thomson range of the present cytosine mass spectrum, the strong peak at 16 Thomson may be rationalized in terms of the relative ease of breaking the single N–C(4) bond between the central ring and the amino group (NH_2). The production of

18 Thomson ions is weak in comparison with the mass spectrum reported by NIST [23]. This suggests that the peak may be primarily due to water impurities whose levels can be expected to vary for different measurements.

To the authors' knowledge, the present work provides the first demonstration in the literature of H^+ fragment ion production from gas-phase cytosine. No clear evidence is observed for the formation of H_2^+ ions or any doubly charged fragments in the range from 2 to 11 Thomson.

3.2.3. Thymine

Fig. 5 shows the mass spectrum for single ion production by EC and DI in 80 keV (1.8 v_0) proton collisions with gas-phase thymine. In common with the equivalent results for adenine, cytosine, and uracil [11], the same peaks were observed for electron capture and for direct ionization in the present collisions (Table 4).

In contrast with cytosine, a number of previous experimental studies are available for the ion impact induced ionization of thymine. In particular, Le Padellec et al. [5] report ion production following 100 keV proton impact, while Schlathölter et al. present TOF mass spectra for gas-phase thymine ionized with incident 0.4 v_0 C^{5+} [28], 0.5 v_0 O^{5+} [28], 0.3 v_0 C^+ [40,41], 0.2 v_0 Xe^{8+} [27], 0.2 v_0 Xe^{25+} [41], 0.4 v_0 Xe^{25+} [42], and 0.4 v_0 C^{3+} and C^{6+} [41]. Fig. 5 and the previous ion impact mass spectra provide evidence for ion production within all the possible groups (1–8), although groups 7 and 8 (with respective maxima at 98 and 112 Thomson in the present data) are generally observed to be weak.

de Vries et al. [41] comment that the production of thymine fragment ions with m/q larger than that of the singly ionized C_4N_2 ring (74 Thomson) implies dissociative ionization without the destruction of the ring itself. We agree that the weak 108–115 Thomson band with a maximum at 112 Thomson points to fragmentation around the CH_3 group, notably CH_2 removal with a minor nuclear arrangement to form uracil$^+$. Indeed the net positive charge remaining with the larger fragment in this process is consistent with Jochims et al.'s [21] description of the (thymine$^+$)* precursor with hole localization on the N(1) atom. Although neither Jochims et al. [21] nor Rice et al. [37] report ion production in this m/q range in their respective 20 eV photo-ionization and 70 eV (2.3 v_0) electron impact experiments, a weak peak is apparent at 112 Thomson in Imhoff et al.'s [39] 70 eV electron impact mass spectrum of gas-phase thymine.

The 95–100 Thomson group observed in the present work with a maximum at 98 Thomson (97 Thomson in the previous high-resolution electron impact and photo-ionization experiments [21,37,39]) is tentatively associated with CH_2N by Jochims et al. [21], presumably following cleavage of the C(2)–N(1) and C(6)–C(5) single bonds of metastable (thymine$^+$)*. The weakness of the peak may be partially explained by hole localization on the N(1) atom of (thymine$^+$)* tending to leave the larger fragment neutral. This proposal appears to be consistent with the strong peak at 28 Thomson, although direct CH_2N^+ loss from (thymine$^+$)* is also identified as a major reaction pathway [21,37,39].

Jochims et al. [21] associate the relatively strong group 6 with the loss of HCNO following the rupture of the N(1)–C(2) and N(3)–C(4) bonds, which are single in both thymine and (thymine$^+$)*. This assignment is supported by Imhoff *et al.*'s [39] analysis of thymine-methyl-d_3-6-d (CH_3 and CH in thymine replaced with CD_3 and CD, respectively) ionization by 70 eV electrons. The local maximum at 83 Thomson in the 20 eV photo-ionization and 70 eV electron impact mass spectra [21,37,39] is presumably due to the lower appearance energy of $C_4H_5NO^+$ (10.7 eV) than $C_4H_4NO^+$ (13.2 eV). Conversely, the group maximum at 82 Thomson in Fig. 5 suggests that $C_4H_5NO^+$, identified by Jochims et al. [21] as an intermediate state in a number of key reaction pathways, may be relatively short-lived in the present proton impact experiments due to the tendency for higher energy deposition.

The group 5 maximum occurs at 70 Thomson in Fig. 5 and in the previous 70 eV electron impact data [37,39], whereas the local maximum for 20 eV photo-ionization maximum is reported at 71 eV [21]. Jochims et al.'s [21] assignment of the respective peaks to $C_2HNO_2^+$ and $C_2H_2N_2O^+$ with entirely separate reaction pathways appears to be consistent with the relative intensities varying according to the ionizing interaction. The group is not visible in Rice et al.'s [37] 20 eV electron impact result.

The peak structure between 20 and 60 Thomson (groups 2–4) in Fig. 5 is generally consistent with the previous ion impact [41], 70 eV electron impact [37,39] and 20 eV photo-ionization mass spectra [21]. The work of Jochims et al. [21] provides a thorough review of the fragmentation pathways. The only apparent differences between the present and previous studies in this m/q range [21,37,39] relate to group 3 (37–45 in the present work). In particular, whereas we observe a local maximum at 43 Thomson, the previous results show increased ion production at 44 Thomson [21,37,39]. These peaks are assigned to $HCNO^+$ [21,39,41], H_2CNO^+ [39], and to CO_2^+ due to an impurity in the beam [21].

Whereas the 80 keV (present work) and 100 keV [5] proton impact data show the local maximum at 43 Thomson to be more intense than its 39 Thomson counterpart, the opposite relation is observed for 70 eV electron impact [39], 0.28–0.45 v_0 C^{n+} (n = 1 and 3) impact [40,41], and 20 eV photo-ionization [21]. $HCNO^+$ production (43 Thomson) is attributed to a charge reversal in the fragmentation associated with group 6 by Jochims et al. [21] and identified as the first step in the most important pathways for sequential fragmentation following ionization. This presumably occurs primarily through the cleavage of the C(2)–N(3) and C(4)–C(5) bonds, tending to leave the larger fragment charged due to hole localization on the N(1) atom in the metastable (thymine$^+$)* precursor. Conversely, breaking the (thymine$^+$)* bonds C(2)–N(3) and N(1)═(6) (single bonded in neutral thymine) would tend to produce $HCNO^+$. As cleaving the N(1)═C(6) double bond will require greater energy transfer, the latter pathway is expected to be relatively probable in the present collisions. By contrast, $C_3H_3^+$ (39 Thomson) production occurs via a sequence of three fragmentations with considerable atomic scrambling. Therefore we propose that this channel may be suppressed in the present measurements compared to the 70 eV electron impact [39] and 20 eV photo-ionization data [21] due to the tendency for more rapid fragmentation following high-energy deposition. Comparisons with de Vries et al.'s [41] C^{n+} (n = 1, 3, and 6) impact data are complicated by interactions with the projectiles' bound electrons. Stronger peaks at 43 and 44 Thomson than at 39 Thomson in the previous highly charged ion impact mass spectra (C^{5+}, C^{6+}, O^{6+}, Xe^{8+}, and Xe^{25+}) [27,28,41,42] can be rationalized in terms of relatively large cross-sections for multi-ionization and the significant production of (43, 82) and (44, 82) Thomson ion pairs observed in de Vries et al.'s [41] coincidence experiments.

As mentioned in section 3.2.II, Imhoff et al.'s [39] electron impact ionization experiments on deuterated thymine provide evidence for CO^+ (28 Thomson) production from gas-phase thymine. Accordingly, while the intense group 2 is mainly associated with CNH_n^+ (n = 1–3) ions following Jochims et al.'s [21] analysis, CO^+ and $C_2H_n^+$ (n = 1–3) product ions are also expected to contribute to the 80 keV proton impact mass spectrum shown in Fig. 5.

The present thymine mass spectrum includes a distinct yet fairly weak peak at 18 Thomson, whereas the group maximum occurs at this m/q for 70 eV electron impact ionization [39]. The relatively slow ion impact measurements of Schlathölter et al. [28,40,41] also show strong ion production at 18 Thomson. To clarify assignments, Imhoff et al. [39] report complimentary experiments on gas-phase thymine-methyl-d_3-6-d (CH_3 and CH in thymine replaced with CD_3

and CD, respectively). In this case the local maximum occurs at 18 Thomson, attributable to CD_3^+ and/or H_2O^+ ions. The authors also report a peak at 20 Thomson, strongly suggesting the formation of D_2O^+ product ions. By analogy, it is probable that the present 18 Thomson peak contains a contribution of H_2O^+ product ions from $(thymine^+)^*$ dissociation. The difference in the relative intensity of the 18 Thomson peak between the present and previous data may be due to changes in the relative contributions of different fragmentation pathways according to the collision conditions and/or to different levels of H_2O impurities in the target beams.

Ion production in the range of 10–20 Thomson following 80 keV proton impact upon thymine shows a local maximum at 15 Thomson. This is consistent with the relatively low energy required to break the single C–C bond joining the CH_3 group to the C_4N_2 ring. Accordingly, Imhoff et al.'s [39] 70 eV electron impact experiments show the 15 Thomson peak to be the most intense in group 1, with the exception of the 18 Thomson peak discussed above. Conversely, Schlathölter et al.'s C^{n+} and O^{5+} impact experiments on gas phase thymine demonstrate the production of C^+ (as well as H_2O^+) to be much stronger than any other ion in the group [28,41]. Particularly in the case of multi-charged ion impact, this difference with the present work may be partially due to double or multiple fragment ion production in single collision events (not counted in the present data). Furthermore, the electronic structure of the projectile is known to play a major role in the ionization dynamics of thymine and uracil [39].

Unlike the results for adenine, cytosine, and uracil [11], the present work reveals clear evidence for ion production at 2 Thomson from gas phase thymine. Strong H_2^+ production is also visible in each of Schlathölter et al.'s ion impact mass spectra (e.g., [41]) and in Imhoff et al.'s 70 eV electron impact data [39]. Additional peaks at 3 and 4 Thomson in Imhoff et al.'s [39] mass spectrum for thymine-methyl-d_3-6-d imply the presence of several competing pathways for H_2^+ production from ionized thymine. Relatively high H_2^+ production may be related to the abundance of C-H bonds (4 in thymine compared to 2 in adenine, cytosine, and uracil), which are weaker than the N–H bonds (see Shukla and Mishra's [43] optimized bond length calculations for nucleobases). Similarly, Table 5 shows the production of H^+ as a percentage of total ionization to be highest for thymine. However, the thymine-methyl-d_3-6-d mass spectrum [39] indicates that the hydrogen atoms from N–H bonds also contribute significantly to H^+ and H_2^+ production from thymine. The analyses of nucleobase dissociative ionization pathways initiated by Rice et al. [26,37] and recently reviewed and developed by Jochims et al. [21] do not extend to the formation of fragment ions <26 Thomson.

3.3. Fragmentation ratios for direct ionization and electron capture

The present experiments enable direct ionization to be compared with electron capture processes in terms of the fragmentation ratios for ion production in a given m/q range against total ionization. Table 5 shows these fragmentation ratios calculated separately for EC and DI (e.g., the number of product ions in a given m/q range produced by EC divided by the total number of product ions produced by EC). The error bars are purely statistical ($n^{-(1/2)}$) and do not take into account the mass spectrometer transmission for different ions. The contribution of background noise could be removed easily as it was observed to be constant for all flight times.

Whereas an incident proton can transfer any amount of its kinetic energy in a single ionizing collision with a molecule (EC or DI), the statistical distribution of ions produced in a large sample of collisions is expected to reflect the specific shape of the energy deposition function corresponding to the nature of the interaction. Naturally, the energy transfer threshold for the production of the *parent ion* is lower than that for dissociative ionization. Therefore, increased fragmentation and greater relative production of small fragment ions (see the appearance energies for adenine, thymine, and uracil fragment ions in Table 1 [21]) provide evidence for a shift towards higher energy deposition. However, it should be noted that deposited energy can also be removed from the molecular system by photon emission or in the form of the KE of an emitted electron, neither of which can be detected in the present experiments.

For all four nucleobases in Table 5, the production of parent ions (given as a percentage of the total ion production) is markedly greater for DI than for EC. This increased tendency for fragmentation following electron capture as compared to direct ionization in 80 keV proton-molecule collisions also occurs for water target molecules [13,14] and is consistent with the association of smaller impact parameters with greater energy transfer. Indeed, Table 1 shows that the probabilities (and therefore cross sections and impact parameters) for EC are distinctly smaller than for DI in the present collisions.

As well as demonstrating that the relative contribution of dissociative ionization is greater for EC than DI, Table 5 shows which m/q ranges account for the additional fragment ions produced by EC. For all four nucleobases in the table, the relative production of H^+ and of ions in groups 2 and 3 is greater for EC than DI[3]. For groups 4–8, relative ion production is either greater for DI than EC or about the same. Therefore the increase in dissociative ionization/total ionization for EC compared with DI is principally associated with the production of *small* or *intermediate* fragment ions ($m/q < 47$), consistent with greater energy deposition in the EC reactions.[1]

It is interesting to consider these results in the context of Alvarado et al.'s [32] comparisons of parent and fragment ion production following singly charged ion and neutral collisions with gas-phase adenine in the velocity range 0.22–0.75 v_0. For ion impact in this velocity regime, ionization occurs dominantly by electron capture, whereas electron capture is very weak for neutral impact at all impact velocities. Moreover, for 0.89–2.45 v_0 collisions with water molecules, the cross-sections for direct ionization by proton impact are similar to the total ionization cross sections for neutral hydrogen impact [13,14,44]. Therefore it is reasonable to draw an approximate analogy between Alvarado et al.'s [32] ion/neutral impact ionization comparisons and the present EC/DI comparisons. As the cross sections (and therefore impact parameters) for electron capture are much larger than those for direct ionization at *low* impact velocities, we would have expected a clear increase in the relative production of fragment ions following neutral impact (analogous to DI) i.e., the opposite trend to the present results. Conversely, Alvarado et al. [32] observed almost no differences in the branching ratios for fragment ion production following H^+ and H^0 impact. This result highlights the potential limitations of the simple association of smaller impact parameters with increased energy deposition as a means to rationalize the ionization-induced fragmentation patterns of electronically complex molecules.

Table 5 shows almost no difference in the relative production of parent ions (given as percentages of total ion production) in 80 keV (1.8 v_0) collisions with adenine, cytosine, and uracil [11]. Thus, despite the differences in the $(nucleobase^+)^*$ relaxation pathways discussed in Section 3.2 and reflected in the relative intensities of the fragment ion groups in Table 5, the overall tendency for the fragmentation of these three molecules is similar under the present ionizing collisions. Only thymine shows distinctly greater fragmentation. The reason for the relative instability of $(thymine^+)^*$ formed in the present collisions is unclear. However, a simple

[1] Ion production in *group 1* should be considered with caution due to suspected water impurities.

comparison of the molecular geometries (Fig. 1) suggests that it may be associated with the availability of (thymine$^+$)* relaxation channels involving the initial removal of the CH_3 group. Indeed, while the fragmentation of (uracil$^+$)*, (cytosine$^+$)*, and (thymine$^+$)* is understood to proceed dominantly through initial HNCO loss [21,37], the detection of ions in groups 7 and 8 demonstrates the contribution of further dissociative ionization pathways. Schlathölter et al. [40] also report greater relative production of fragment ions from thymine than from uracil following 0.28 v_0 C^+ impact.

4. Conclusions

For single ion production following proton impact upon gas-phase adenine, cytosine, and thymine, branching ratios for electron capture/total ionization (direct ionization + electron capture) are reported for the first time and agree closely with previous data for 80 keV (1.8 v_0) proton collisions with uracil [11] and water [13–15]. Separate mass spectra are presented for direct ionization and electron capture for each of the DNA bases studied. The two ionization processes produce the same groups of ions, albeit with different relative intensities. The observed product ions are generally consistent with previous measurements, notably for singly charged ion impact ionization (e.g., [5]), 70 eV electron impact ionization (e.g., [39]), and 20 eV photo-ionization [21]. Several differences with previous mass spectra, e.g., a stronger production of $HCNO^+$ than $C_3H_3{}^+$ in 80 keV proton collisions for thymine as compared to the opposite following 70 eV electron impact [39], can be rationalized on the basis of particularly high energy deposition in the present collisions.

As observed for uracil [11] and water [14], the present fragmentation ratios (fragment ion production divided by total ionization) in 80 keV proton collisions with adenine, cytosine, and thymine are greater following electron capture than direct ionization reactions. This ionization process dependence of DNA base fragmentation patterns highlights the necessity of quantitative experimental measurements (notably fragmentation ratios and absolute cross sections) following projectile collisions with biomolecules in order to model radiation damage on the molecular scale.

Acknowledgements

The *Institut de Physique Nucléaire de Lyon* is part of IN2P3-CNRS, the French national research institute for nuclear and particle Physics. Financial support was provided by the French, Austrian, and Moroccan governments, and by the EU Commission (Brussels) through the Amadee and PICS 2290 programs and the CNRS-CNRST (no. 17689) convention. S. Eden acknowledges an FP6 Marie Curie Fellowship (IEF RADAM-BIOCLUS) and reintegration grant, as well as an EPSRC Life Sciences Interface Fellowship.

References

[1] C. von Sonntag, The Chemical Basis for Radiation Biology, Taylor and Francis, London, 1987.
[2] B. Boudaiffa, P. Cloutier, D. Hunting, M.A. Hues, L. Sanche, Science 287 (2000) 1658.
[3] B. Coupier, B. Farizon, M. Farizon, M.J. Gaillard, F. Gobet, N.V. de Castro Faria, G. Jalbert, S. Ouaskit, M. Carré, B. Gstir, G. Hanel, S. Denifl, L. Feketeova, P. Scheier, T.D. Märk, Eur. Phys. J. D 20 (2002) 459.
[4] P. Moretto-Capelle, A. Le Padellec, Phys. Rev. A 74 (2006) 062705.
[5] A. Le Padellec, P. Moretto-Capelle, M. Richard-Viard, J.P. Champeaux, P. Cafarelli, J. Phys.: Conf. Ser. 101 (2008) 012007.
[6] M. Biaggi, F. Ballarini, W. Burkard, E. Egger, A. Ferrari, A. Ottolenghi, Nucl. Instr. Methods Phys. Res. B 159 (1999) 89.
[7] R. Cabrera-Trujillo, P. Apell, J. Oddershede, J.R. Sabin, Application of Accelerators in Research and Industry International Conference: AIP Conference Proceedings, vol. 680, 2003, p. 86.
[8] V. Periquet, A. Moreau, S. Carles, J.P. Schermann, C. Desfrançois, J. Electron Spectrosc. Relat. Phenom. 106 (2000) 141.
[9] P. Colarusso, K. Zhang, B. Guo, P.F. Bernath, Chem. Phys. Lett. 269 (1997) 39.
[10] E. Nir, M. Müller, L.I. Grace, M.S. de Vries, Chem. Phys. Lett. 355 (2002) 59.
[11] J. Tabet, S. Eden, S. Feil, H. Abdoul-Carime, B. Farizon, M. Farizon, S. Ouaskit, T.D. Märk, Phys. Rev. A 81 (2010) 012711.
[12] H. Luna, C. McGrath, M.B. Shah, R.E. Johnson, M. Liu, C.J. Latimer, E.C. Montenegro, Astrophys. J. 628 (2005) 1086.
[13] F. Gobet, B. Farizon, M. Farizon, M.J. Gaillard, M. Carre, M. Lezius, P. Scheier, T.D. Märk, Phys. Rev. Lett. 86 (2001) 3751.
[14] F. Gobet, S. Eden, B. Coupier, J. Tabet, B. Farizon, M. Farizon, M.J. Gaillard, M. Carré, S. Ouaskit, T.D. Märk, P. Scheier, Phys. Rev. A 70 (2004) 062716.
[15] H. Luna, A.L.F. de Barros, J.A. Wyer, S.W.J. Scully, J. Lecointre, P.M.Y. Garcia, G.M. Sigaud, A.C.F. Santos, V. Senthil, M.B. Shah, C.J. Latimer, E.C. Montenegro, Phys. Rev. A 75 (2007) 042711.
[16] W. Friedland, P. Jacob, P. Bernhardt, H.G. Paretzke, M. Dingfelder, Radiat. Res. 159 (2003) 401.
[17] D. Huber, M. Beikircher, S. Denifl, F. Zappa, S. Matejcik, A. Bacher, V. Grill, T.D. Märk, P. Scheier, J. Chem. Phys. 125 (2006) 084304.
[18] P.D. Burrow, G.A. Gallup, A.M. Scheer, S. Denifl, S. Ptasinska, T.D. Märk, P. Scheier, J. Chem. Phys. 124 (2006) 124310.
[19] S. Denifl, S. Ptasinska, G. Hanel, B. Gstir, P. Scheier, M. Probst, B. Farizon, M. Farizon, S. Matejcik, E. Illenberger, T.D. Märk, Phys. Scr. T110 (2004) 252.
[20] A.B. Trofimov, J. Schirmer, V.B. Kobychev, A.W. Potts, D.M.P. Holland, L. Karlsson, J. Phys. B: At. Mol. Opt. Phys. 39 (2006) 305.
[21] H.-W. Jochims, M. Schwell, H. Baumgärtel, S. Leach, Chem. Phys. 314 (2005) 263.
[22] D. Dougherty, E.S. Younathan, R. Voll, S. Abdulnur, S.P. McGlynn, J. Electron Spectrosc. Relat. Phenom. 13 (1978) 379.
[23] NIST Chemistry WebBook, available from http://webbook.nist.gov/.
[24] D. Lafaivre, P. Marmet, Can. J. Phys. 56 (1978) 1549.
[25] J.D. Morrison, J.C. Traeger, Int. J. Mass Sprectrom. Ion Phys. 11 (1973) 77.
[26] J.M. Rice, G.O. Dudek, J. Am. Chem. Soc. 89 (1967) 2719.
[27] T. Schlathölter, F. Alvarado, S. Bari, R. Hoekstra, Phys. Scr. 73 (2006) C113.
[28] T. Schlathölter, F. Alvarado, S. Bari, A. Lecointre, R. Hoekstra, V. Bernigaud, B. Manil, J. Rangama, B. Huber, ChemPhysChem 7 (2006) 2339.
[29] R. Brédy, J. Bernard, L. Chen, B. Wei, A. Salmoun, T. Bouchama, M.C. Buchet-Poulizac, S. Martin, Nucl. Instr. Methods Phys. Res. B 235 (2005) 392.
[30] R. Cabrera-Trujillo, Y. Öhrn, E. Deumens, J.R. Sabin, Phys. Rev. A 62 (2000) 052714.
[31] R. Abouaf, H. Dunet, Eur. Phys. J. D 35 (2005) 405.
[32] F. Alvarado, S. Bari, R. Hoekstra, T. Schlathölter, J. Chem. Phys. 127 (2007) 034301.
[33] M. Schwell, H.-W. Jochims, H. Baumgartel, F. Dulieu, S. Leach, Planetary Space Sci. 54 (2006) 1073.
[34] J.L. Occolowitz, Chem. Commun. (1968) 1226.
[35] M.G. Barrio, D.I.C. Scopes, J.B. Holtwick, N.J. Leonard, Proc. Natl. Acad. Sci. U.S.A. 78 (1981) 3986.
[36] S.K. Sethi, S.P. Gupta, E.E. Jenkins, C.W. Whitehead, L.B. Townsend, J.A. McCloskey, J. Am. Chem. Soc. 104 (1982) 3349.
[37] J.M. Rice, G.O. Dudek, M. Barber, J. Am. Chem. Soc. 87 (1965) 4569.
[38] S.K. Kim, W. Lee, D.R. Herschbach, J. Phys. Chem. 100 (1996) 7933.
[39] M. Imhoff, Z. Deng, M. Huels, Int. J. Mass Spectrom. 245 (2005) 68.
[40] T. Schlathölter, F. Alvarado, R. Hoekstra, Nucl. Instr. Methods Phys. Res. B 223 (2005) 62.
[41] J. de Vries, R. Hoekstra, R. Morgenstern, T. Schlathölter, Phys. Scr. T110 (2004) 336.
[42] T. Schlathölter, R. Hoekstra, R. Morgenstern, Int. J. Mass Spectrom. 233 (2004) 173.
[43] M.K. Shukla, P.C. Mishra, Chem. Phys. 240 (1999) 319.
[44] F. Gobet, S. Eden, B. Coupier, J. Tabet, B. Farizon, M. Farizon, M.J. Gaillard, S. Ouaskit, M. Carré, T.D. Märk, Chem. Phys. Lett. 421 (2006) 68.